J. Meas. Sci. Instrum., 2024, 15(3): 292-301.
DOI: 10.62756/jmsi.1674-8042.2024030
http://jmsi.publish.founderss.cn
jmsi@nuc.edu.cn

Asymmetrical Fabry-Perot cavity slot micro-ring resonator and its sensing characteristics

CAO Qianqian, LIU Chunjuan*, WU Xiaosuo, SUN Xiaoli

School of Electronic and Information Engineering, Lanzhou Jiaotong University, Lanzhou 730070, China

***Corresponding author:** LIU Chunjuan (liuchj@mail.lzjtu.cn)

Received: April 10, 2024 **Revised:** June 21, 2024 **Accepted:** June 25, 2024

Abstract: To achieve high quality factor and high-sensitivity refractive index sensor, a slot micro-ring resonator (MRR) based on asymmetric Fabry-Perot (FP) cavity was proposed. The structure consisted of a pair of elliptical holes to form an FP cavity and a micro-ring resonator. The two different optical modes generated by the micro-ring resonator were destructively interfered to form a Fano line shape, which improved the system sensitivity while obtaining a higher quality factor and extinction ratio. The transmission principle of the structure was analyzed by the transfer matrix method. The transmission spectrum and mode field distribution of the proposed structure were simulated by the finite difference time domain (FDTD) method, and the key structural parameters affecting the Fano line shape in the device were optimized. The simulation results show that the quality factor of the device reached 22 037.1, and the extinction ratio was 23.9 dB. By analyzing the refractive index sensing characteristics, the sensitivity of the structure was 354 nm·RIU^{-1}, and the detection limit of the sensitivity was 2×10^{-4} RIU. Thus, the proposed compact asymmetric FP cavity slot micro-ring resonator has obvious advantages in sensing applications owing to its excellent performance.

Key words: micro-ring resonator (MRR); Fabry-Perot (FP) cavity; Fano resonance; refractive index sensing; integrated optics; silicon waveguide

0 Introduction

Silicon on insulator (SOI) technology plays an important role in today's optoelectronic communication field[1]. Owing to the characteristics of full compatibility with CMOS process and high refractive index, SOI is helpful to realize new optical devices with strong mode field strength and small waveguide bending radius[2,3].

In a myriad of optical devices built on SOI materials, the micro-ring resonator (MRR) has attracted significant attention owing to its compact structure, low power consumption, and high integration capability. It has been widely used in biomedicine[4,5], environmental monitoring[6], food safety[7,8], refractive index sensing and other fields. However, the existing MRRs may cause periodic attenuation of the resonance line shape in the transmission spectrum through side-coupled bus waveguide[9], which is crucial to the sensing performance of MRR-based sensors[10]. In the realm of sensing applications utilizing MRRs, although the conventional symmetrical Lorentzian line shape can attain a high quality factor (Q), it suffers from drawbacks such as a small slope of resonance peak and a low extinction ratio[11,12]. In recent years, researchers have been working on adjusting the traditional Lorentzian line to other types of resonance lines. For example, in the MRR waveguide under specific coupling conditions, the Lorentzion line shape in the transmission spectrum is adjusted to an asymmetric Fano line shape, which features a steeper slope rate and a much narrower range of 0—1 for tuning transmission. These characteristics substantially enhance its power consumption, sensing sensitivity and extinction ratio, thereby significantly boosting the sensor's performance[13-15]. Therefore, many structures that can generate Fano resonance and be used in the sensing field have been proposed. Peng et al.[16] realized a Q factor of up to 32 000 by coupling a photonic crystal cavity with a micro-ring, but its sensitivity was only 67 nm·RIU^{-1}. Gao et al.[17] used a runway-type micro-ring sensor with two air holes inserted in the side-coupled waveguide, achieving a remarkable extinction ratio of 53.09 dB, albeit with a sensitivity of merely 125 nm·RIU^{-1}. Liu et al.[18] introduced a sensing structure based on slot Bragg grating coupled micro-rings, boasting a Q value of 25 729, yet achieving a sensitivity of only

122 nm·RIU^{-1}. Additionally, Wen et al.[19] proposed a full-grating racetrack resonator based on sub-wavelength gratings, which had a sensitivity of up to 500 nm/RIU, but its structure was relatively complex. Therefore, on the premise of ensuring the small size and simple structure of the device, how to achieve high Q value and high sensitivity by realizing Fano resonance is still an important issue in the sensing application of micro-ring resonators.

In this study, a structure of micro-ring resonator based on asymmetric Fabry-Perot(FP) cavity was proposed. The reflection of the optical signal was realized by inserting two elliptical holes into the bus waveguide to form an FP cavity. The continuous state optical mode generated by the FP cavity and the discrete state optical mode generated by MRR interfered with each other to generate Fano line shape, so that high Q factor and high sensitivity were achieved simultaneously in a small volume. To optimize the Fano line shape, the structural parameters such as the FP cavity length and the long axis radius of the hole were optimized by the finite difference time domain(FDTD) method, and the sensing performance of the device was analyzed.

1 Basic principle

1.1 Structure design

The three-dimensional structure of an asymmetrical FP cavity slot micro-ring resonator(AFPSMRR) is shown in Fig.1(a), which consists of a straight waveguide with FP cavity and a slot micro-ring resonator. As shown in Fig.1(b), a pair of elliptical holes with the same size are etched on the bus waveguide to form an FP cavity. The cavity length of the FP cavity is $L=L_{C1}+L_{C2}$, the radius of the micro-ring is $R=5.5$ μm, and the long and short half axes of the elliptical pores are R_C and r_C, respectively. The main parameters of the device also include the bus waveguide width W_0, the coupling gap W_{gap} and the slot width W_{slot}. The coupling gap W_{gap} and the slot width W_{slot} are 212 nm and 58 nm, respectively. The structure is based on the SOI material, with a 220 nm thick waveguide layer, and the thickness of the silicon dioxide substrate is 2 μm.

By inserting a pair of elliptical holes in the bus waveguide, the utilization of light and the coupling ability between the waveguide and the micro-ring are improved. Since the distance between the two holes is large enough, the partial reflector which makes the hole as the propagation mode in the bus waveguide can be regarded as an FP cavity[20]. When the optical signal enters the bus waveguide, the continuous resonance mode with phase delay caused by the reflection of the FP cavity will destructively interfere with the discrete waveguide mode generated by the MRR, forming an asymmetric Fano line. The asymmetric Fano line can provide extremely narrow resonance linewidth and high extinction ratio. In addition, elliptical holes have fewer manufacturing defects than rectangular or triangular holes and lower insertion loss than that of circular holes[21].

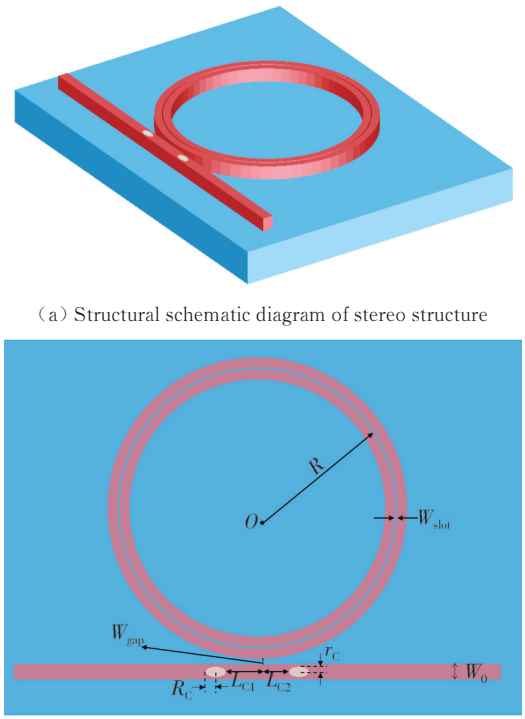

(a) Structural schematic diagram of stereo structure

(b) Top view and structural parameters

Fig. 1 Structure diagram of AFPSMRR

1.2 Theoretical analysis

The theoretical model of the designed AFPSMRR is shown in Fig.2.

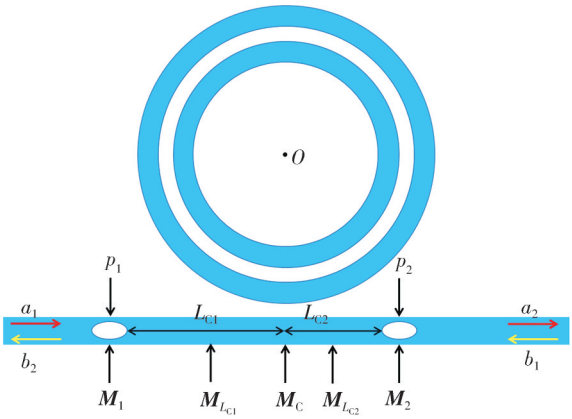

Fig. 2 Theoretical model of AFPSMRR

Transmission matrix analysis is performed on the model. The elliptical hole has forward and backward propagation modes along the bus waveguide, where a_1 and b_1 are the amplitude of the incident light field on the left and right

sides, a_2 and b_2 are the amplitude of the transmitted light field and the amplitude of the reflected light field at the output end, respectively. The relationship between them can be expressed as

$$\begin{bmatrix} a_2 \\ b_1 \end{bmatrix} = \boldsymbol{M}_{\mathrm{AFP}} \begin{bmatrix} a_1 \\ b_2 \end{bmatrix}, \tag{1}$$

where $\boldsymbol{M}_{\mathrm{AFP}}$ is the total transmission matrix of the system. Since the proposed scheme consists of a straight waveguide L_{C1}, a slot micro-ring resonator, a straight waveguide L_{C2}, and a partial reflector composed of elliptical holes p_1 and p_2, the total transfer matrix of the whole structure can be expressed as

$$\boldsymbol{M}_{\mathrm{AFP}} = \boldsymbol{M}_1 \boldsymbol{M}_{L_{\mathrm{C1}}} \boldsymbol{M}_{\mathrm{C}} \boldsymbol{M}_{L_{\mathrm{C2}}} \boldsymbol{M}_2, \tag{2}$$

where $\boldsymbol{M}_1$ is the transmission matrix of the elliptical hole p_1; $\boldsymbol{M}_{L_{\mathrm{C1}}}$ is the transmission matrix of the straight waveguide with a length of L_{C1}; $\boldsymbol{M}_{\mathrm{C}}$ is the transmission matrix of the slot micro-ring resonator; $\boldsymbol{M}_{L_{\mathrm{C2}}}$ is the transmission matrix of the straight waveguide with a length of L_{C2}; and $\boldsymbol{M}_2$ is the transmission matrix of the elliptical hole p_2. If the reflection coefficient of the hole is set to be r_{p}, the transmission matrix of the elliptical hole as part of the reflector is

$$\boldsymbol{M}_p = \frac{1}{\mathrm{i}\sqrt{1-r_p^2}} \begin{bmatrix} -1 & -r_p \\ r_p & 1 \end{bmatrix}, \tag{3}$$

where $p=1, 2$. When the light propagates in the FP cavity composed of two holes, the transmission matrices are

$$\boldsymbol{M}_{L_{\mathrm{C1}}} = \begin{bmatrix} \mathrm{e}^{-\mathrm{i}\varphi_1} & 0 \\ 0 & \mathrm{e}^{\mathrm{i}\varphi_1} \end{bmatrix}, \tag{4}$$

$$M_{L_{\mathrm{C2}}} = \begin{bmatrix} \mathrm{e}^{-\mathrm{i}\varphi_2} & 0 \\ 0 & \mathrm{e}^{\mathrm{i}\varphi_2} \end{bmatrix}, \tag{5}$$

where φ_1 and φ_2 are used to describe the phase difference caused by holes p_1 and p_2 respectively when the optical signal propagates for a week in the device. Here, $\varphi_1 = 2\pi n L_{\mathrm{C1}}/\lambda$, $\varphi_2 = 2\pi n L_{\mathrm{C2}}/\lambda$, λ is the working wavelength, and n is the effective refractive index of the propagation mode.

After the light propagates through the coupling point, the transmission spectrum is

$$t_{\mathrm{C}}(\lambda) = \frac{\mu - a\exp(\mathrm{i}2\pi n L_{\mathrm{C}}/\lambda)}{1 - \mu a \exp(\mathrm{i}2\pi n L_{\mathrm{C}}/\lambda)}, \tag{6}$$

where μ is the transmission coefficient of the coupling region of the device. In addition, when the loss coefficient of the light propagating in the micro-ring with a circumference of L_{C} is α, the round-trip amplitude is $a = \mathrm{e}^{-\alpha L_{\mathrm{C}}}$. The transfer matrix of the slot micro-ring resonator is

$$\boldsymbol{M}_{\mathrm{C}} = \begin{bmatrix} t_{\mathrm{C}} & 0 \\ 0 & t_{\mathrm{C}}^{-1} \end{bmatrix}. \tag{7}$$

Therefore, combined with Eqs. (1) — (7), the transmission matrix of the whole asymmetric FP cavity slot micro-ring resonant coupling structure can be obtained by

$$\begin{bmatrix} a_2 \\ b_1 \end{bmatrix} = \frac{1}{\mathrm{i}\sqrt{1-r_1^2}} \begin{bmatrix} -1 & -r_1 \\ r_1 & 1 \end{bmatrix} \begin{bmatrix} \mathrm{e}^{-\mathrm{i}\varphi_1} & 0 \\ 0 & \mathrm{e}^{\mathrm{i}\varphi_1} \end{bmatrix} \times \begin{bmatrix} t_{\mathrm{C}} & 0 \\ 0 & t_{\mathrm{C}}^{-1} \end{bmatrix} \begin{bmatrix} \mathrm{e}^{-\mathrm{i}\varphi_2} & 0 \\ 0 & \mathrm{e}^{\mathrm{i}\varphi_2} \end{bmatrix} \frac{1}{\mathrm{i}\sqrt{1-r_2^2}} \begin{bmatrix} -1 & -r_2 \\ r_2 & 1 \end{bmatrix} \begin{bmatrix} a_1 \\ b_2 \end{bmatrix}. \tag{8}$$

When the optical signal is only input from the left side of the bus waveguide, that is, $a_1=1$, $b_1=0$ in Eq. (8). The normalized transmittance of the slot micro-ring resonator based on the asymmetric FP cavity can be obtained as

$$T(\lambda) = \left| \frac{a_2}{a_1} \right|^2 = \left| \frac{\sqrt{1-r_1^2}\sqrt{1-r_2^2}\, t_{\mathrm{C}} \mathrm{e}^{\mathrm{i}(\varphi_1+\varphi_2)}}{1 - r_1 r_2 \mathrm{e}^{2\mathrm{i}(\varphi_1+\varphi_2)} t_{\mathrm{C}}^2} \right|^2. \tag{9}$$

To further describe the coupling relationship between the FP cavity and the micro-ring resonator, let $\varphi = \varphi_1 + \varphi_2$, $L = L_{\mathrm{C1}} + L_{\mathrm{C2}}$, Eq. (9) is equivalent to

$$T(\lambda) = \left| \frac{\sqrt{1-r_1^2}\sqrt{1-r_2^2}}{1 - r_1 r_2 \mathrm{e}^{2\mathrm{i}\varphi}} \right|^2 |t_{\mathrm{C}}|^2 \left| \frac{1 - r_1 r_2 \mathrm{e}^{2\mathrm{i}\varphi}}{1 - r_1 r_2 \mathrm{e}^{2\mathrm{i}\varphi} t_{\mathrm{C}}^2} \right|^2 = T_{\mathrm{AFP}} T_{\mathrm{SMRR}} T_{\mathrm{in}}, \tag{10}$$

where $\varphi = 2\pi n L/\lambda$, representing the total phase difference caused by the reflection units p_1 and p_2 as partial reflectors, T_{AFP} represents the transfer function of the asymmetric FP cavity, T_{SMRR} represents the transfer function of the slot micro-ring resonator, and T_{in} represents the coupling transfer function between the FP cavity and the slot micro-ring resonator. When $\mu=1$, Eq. (10) is simplified as

$$T(\lambda) = \left| \frac{\sqrt{1-r_1^2}\sqrt{1-r_2^2}}{1 - r_1 r_2 \mathrm{e}^{2\mathrm{i}\varphi}} \right|^2. \tag{11}$$

As a result, there is only the transmission spectrum of the straight waveguide containing the FP cavity, and Fig. 3(a) is the transmission spectrum in this state. When the reflection coefficient of the hole is $r_1=r_2=0$, the normalized transmittance of AFPSMRR is simplified as

$$T(\lambda) = |t_{\mathrm{C}}|^2. \tag{12}$$

Eq. (12) means that there is only the coupling output of the slot micro-ring resonator cavity and the straight waveguide in the transmission spectrum of the device. The transmission spectrum in this state is shown in Fig.3(b), which is the Lorentzian spectrum.

When the continuous state and the narrow and symmetric discrete state are coupled through different

paths, quantum interference occurs, and the broadband resonance generated by the FP cavity is more likely to overlap with the narrowband resonance of the MRR, resulting in asymmetric linear Fano resonance. According to the Fano spectral line formula $T=1-(q+\gamma)^2/(1+\gamma^2)$ [22,23] (γ is the reduced frequency) for fitting, the asymmetric parameter $q=\cot\varphi$. Due to the existence of reverse transmission light in the coupling process, side peaks may appear in the Fano line shape.

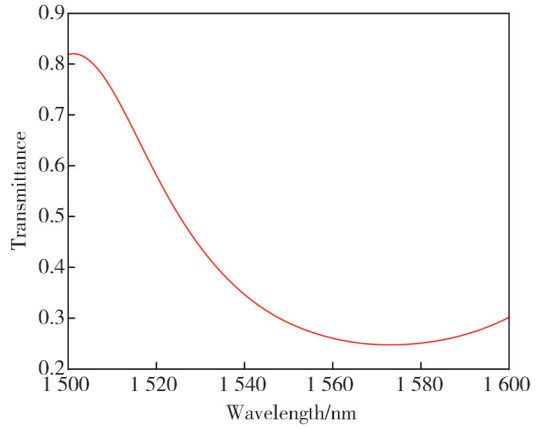

(a) Asymmetric FP cavity

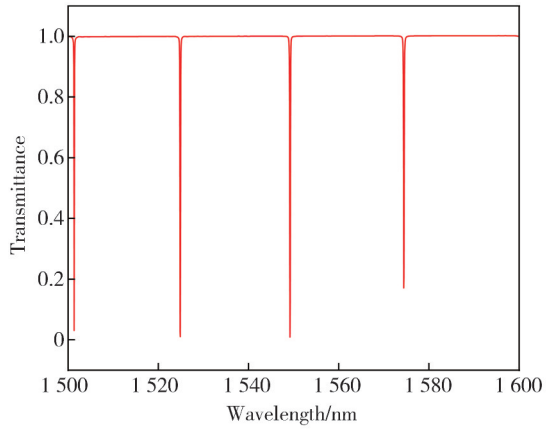

(b) Slot micro-ring resonator

Fig. 3 Transmission spectra of asymmetric FP cavity and slot micro-ring resonator

2 Results and discussion

The Lumerical Mode Solutions software was used to model and simulate the mode field distribution of the proposed device structure and the transmission spectrum under different structural parameters.

2.1 Simulation

The incident light wavelength was selected to be within 1 500 nm — 1 600 nm, the quasi-TE mode was injected into the bus waveguide. The background refractive index was 1.333, the bus waveguide width was 400 nm, and the bending waveguide width is 272 nm. The reflection signal produced by the elliptical hole is coupled with the slot micro-ring to generate a line shape, as illustrated in Fig. 4. It can be seen that the waveguide mode is non-resonant with the FP cavity, and it resonates with the MRR. Fano line shape is generated in the range of the resonance peak to the resonance valley of the FP cavity transmission spectrum. The following analysis focuses on the Fano lineshape within a spectrum range of 1 530 nm — 1 560 nm.

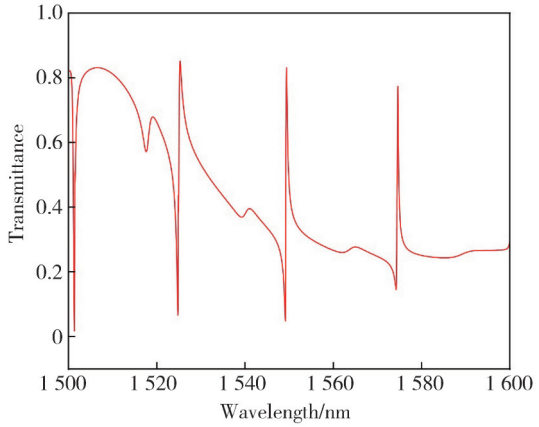

Fig. 4 Transmission spectrum of AFPSMRR

The mode field distribution of the slot waveguide is depicted in Fig. 5. As shown in Fig. 5(a), the optical signal can be entirely confined within the low-emissivity slit region. Compared to the rectangular waveguide of identical dimensions depicted in Fig. 5(b), there is a reduction in light scattering loss and an enhancement in light-confinement capability. In optical refractive index sensing applications, the slot structure is exposed to the external environment, while the substance to be detected is covered and fills the slit. This arrangement facilitates a better interaction between the light and the substance to be detected, with the objective of augmenting the sensor's sensitivity to changes in the refractive index of the detected object.

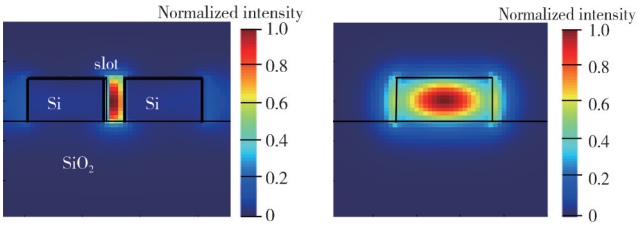

(a) Slot waveguide (b) Strip waveguide

Fig. 5 Mode field distribution of different waveguides in the same size

2.2 Optimization of parameters

For the proposed AFPSMRR device, the FP cavity composed of two elliptical holes is an important part. The cavity length (L), hole position and its long axis

radius (R_C) affect the mutual interference between the FP cavity waveguide and the micro-ring resonator.

Firstly, the position of hole p_2 is fixed, and the L_{C2}=1 μm is kept unchanged. Only the length L_{C1} of the hole p_1 from the center of the coupling point is adjusted to control the FP cavity length, and the influence of the FP cavity length on the sensing performance of the device is analyzed. The other parameters of the device are as follows: R_C=160 nm, and r_C=100 nm. The influence of the FP cavity length on the Fano resonance spectrum is shown in Fig.6 (a).

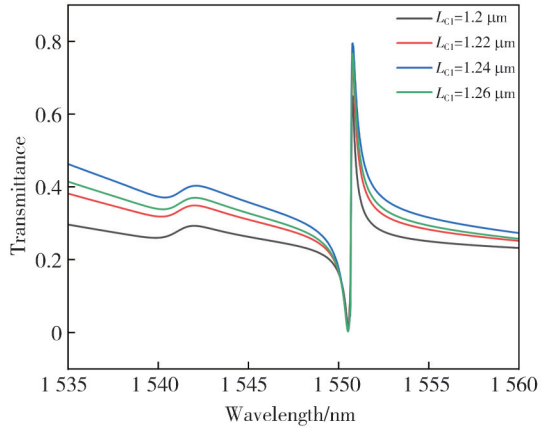

(a) Spectrum lines of Fano resonance at different L_{C1}

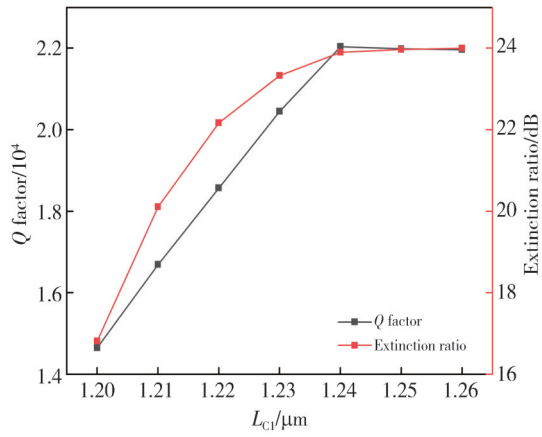

(b) Extinction ratio and Q factor at different L_{C1}

Fig. 6 Changes of transmission spectrum and Fano resonance line shape of asymmetric FP cavity at different L_{C1}

It can be found that as L_{C1} decreases, the resonance peak gradually decreases, which means that too small value of the FP cavity length may reduce the amplitude of the Fano spectrum. This is also because the wavelength of the FP cavity resonance peak may shift with the change of the asymmetric FP cavity length. As shown in Fig.6 (b), when L_{C1} increases, the Q factor and extinction ratio also increase. When L_{C1}=1.24 μm, the Q factor and extinction ratio are 22 037.1 and 23.9 dB, respectively, because the increase of the FP cavity length improves the coupling ability between the FP cavity and the micro-ring resonator. In principle, the longer the FP cavity length, the better the sensing performance of the device. Because there is usually waveguide loss in the process of light transmission, the FP cavity length exceeding a certain length may make the sensor performance worse. From Fig. 6 (b), it can also be clearly seen that Q factor begins to decrease after L_{C1} exceeds 1.24 μm. Therefore, the FP cavity length is determined to be 2.24 μm to maintain a high Q factor for the device.

In Fig.7, the transmission spectra of the device with two holes at different positions are shown while keeping the hole distance L (2.24 μm) unchanged. As holes p_1 and p_2 shift to the left, i.e., L_{C1} increases from 1 μm to 1.32 μm, and L_{C2} decreases from 1.24 μm to 0.92 μm, the transmittance of the Fano resonance line gradually rises.

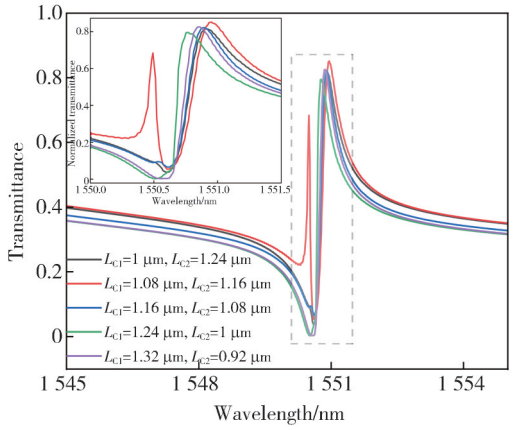

(a) Fano resonance spectral lines at different hole positions

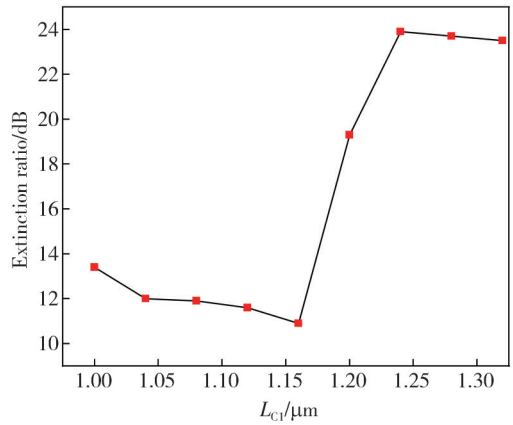

(b) Extinction ratio at different hole positions

Fig. 7 Fano resonance lines of two holes at different positions with L unchanged

During this process, the Fano line exhibits a side peak, which demonstrates an initial increase followed by a decrease. Notably, when L_{C1} and L_{C2} are 1.24 μm and 1 μm, respectively, the minimum value of the Fano spectral line approaches zero, indicating that the FP cavity and the slot micro-ring approach the critical

coupling state. It can be clearly seen from Fig.7(a) that the slope of the Fano spectral line reaches its maximum in this state. However, as the hole continues to shift leftward, the spectral slope diminishes. This phenomenon occurs because the slight leftward movement of the hole enhances the reflection effect of the FP cavity on light, enabling more light to couple into the slot micro-ring, and resulting in an increase in the peak value of the side peak. When hole p_1 is positioned too close to the incident light, some light will be reflected back to the input end by p_1, weakening the coupling effect between the FP cavity and the slot micro-ring, and gradually causing the side peak to disappear. It can be shown from Fig. 7(b) that the extinction ratio peaks when the hole position shifts to L_{C1}=1.24 μm and L_{C2}=1 μm. This further confirms that the device is approaching the critical coupling state more closely when the hole is positioned at this location. At this point, the two holes are asymmetric about the coupling center.

To further explain the coupling state of the hole at different positions, the FDTD method was used to simulate the magnetic field distribution of Z direction at the trough of the Fano resonance spectrum when the hole positions (L_{C1}, L_{C2}) were (1 μm, 1.24 μm), (1.08 μm, 1.16 μm), (1.24 μm, 1 μm), respectively. The results are presented in Fig.8, and the propagation path of light and its coupling interactions can be observed. It is noted that when the hole position is solely at (1.24 μm, 1 μm) as illustrated in Fig. 8(a), no light is transmitted out from the straight end, resulting in a zero transmission phenomenon in the transmission spectrum. This observation also elucidates why the minimum value of the Fano spectral line is nearly zero when the hole is at this position in Fig. 7(a). When the hole position is located at (1.08 μm, 1.16 μm) in Fig. 8(b), the magnetic field distribution of the straight waveguide weakens compared to that in Fig. 8(a) and Fig. 8(c). This implies that more light is localized in the slot micro-ring resonator, and the coupling light returned to the bus waveguide cancels out with the straight light. The excess coupling light will be output from the straight end of the device, indicating that the coupling effect between the FP cavity and the slot micro-ring is strong in this case. The light far from the resonant wavelength will also be coupled into the slot micro-ring, prompting more reverse transmission light to be added to the coupling of the micro-ring resonator and the FP cavity, and resulting in the appearance of the side peak of the Fano line when the hole is located at (1.08 μm, 1.16 μm) position in Fig. 7(a). Compared with Fig. 8(a) and Fig.8(b), when the hole is located at (1 μm, 1.24 μm), due to the weak reflection of the FP cavity, the direct light and the coupled light cannot be completely offset, resulting in a small amount of direct light output along the bus waveguide.

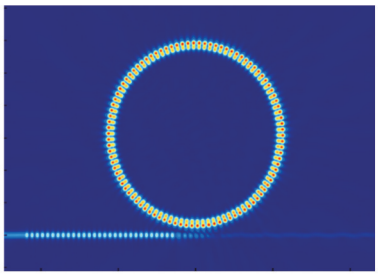

(a) H_Z field distribution at the trough of (1 μm, 1.24 μm)

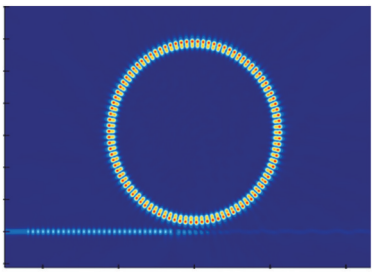

(b) H_Z field distribution at the trough of (1.08 μm, 1.16 μm)

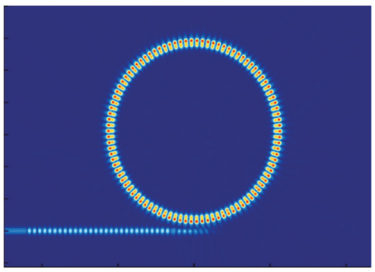

(c) H_Z field distribution at the trough of (1.24 μm, 1 μm)

Fig. 8 Magnetic field distribution of Fano resonance spectral line trough at different positions of hole

Aside from the cavity length and hole position, the reflection ability of the elliptical holes that constitute the FP cavity is also an important factor affecting the performance of the sensor. In addition, the size of the hole will indirectly affect the cavity length of the FP cavity. Fig. 9(a) shows the change of the transmission spectrum of the asymmetric FP cavity when the long axis radius of the elliptical hole increases from 140 nm to 200 nm. It can be seen that with the increase of the long axis radius of the hole, the transmittance of the spectral line shows a decreasing trend, which means that the long axis radius of the hole is positively correlated with the reflection coefficient of the reflector. In addition, the resonance peak of the asymmetric FP cavity is red-shifted with the increase of R_C, which is caused by the change of the long axis radius of the hole affecting the cavity length of the FP cavity. Fig.9(b) is the influence

of the long radius R_C of different elliptical holes on the output Fano line shape while other parameters of the device remain unchanged. With the increase of R_C, the resonance peak decreases, and the Fano line has a side peak at R_C=200 nm. This is because the increase of R_C increases the reflection coefficient of the reflector, which makes the reflected light stronger.

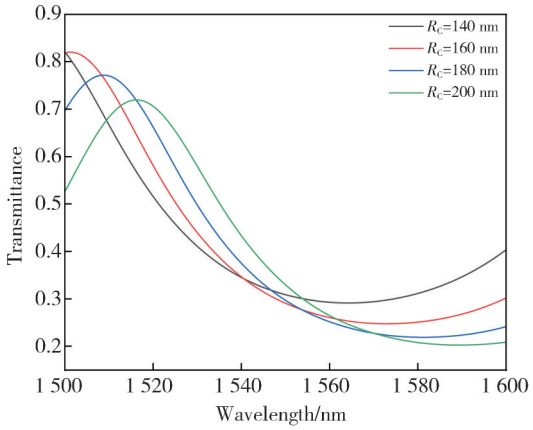

(a) Transmission spectra of asymmetric FP cavity at different R_C

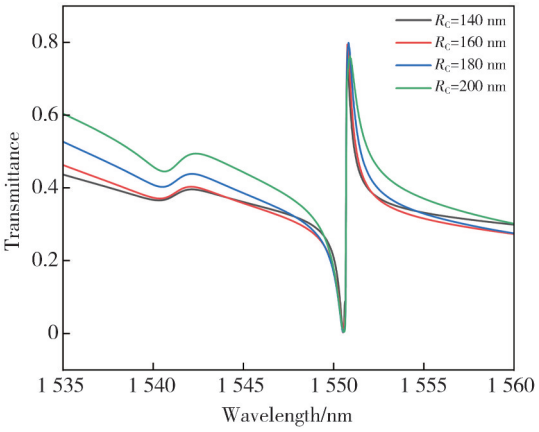

(b) Fano resonance line shapes at different R_C

Fig. 9 Changes of transmission spectrum and Fano resonance lineshape of asymmetric FP cavity at different R_C

Fig. 10 shows the relationship between R_C and Q factor. It can be seen that Q factor increases slowly with the increase of R_C, but when R_C increases to 160 nm, Q factor decreases sharply. The main reason is that the increase of R_C indirectly leads to the decrease in the length of the FP cavity, which changes the position of the resonance peak of the asymmetric FP cavity, thus weakening the interference ability of the FP cavity and the micro-ring resonator. Q factor has a maximum value of 22 037.1 at 160 nm, so the long axis radius of the elliptical hole in the simulation is determined to be 160 nm. Although it is difficult to control the size of the elliptical hole in the process of manufacturing, Kathleen et al.[24] completed the preparation of circular holes with a radius of only 85 nm using deep ultraviolet lithography technology. Therefore, the process preparation conditions required for the device can be completed with the existing technology.

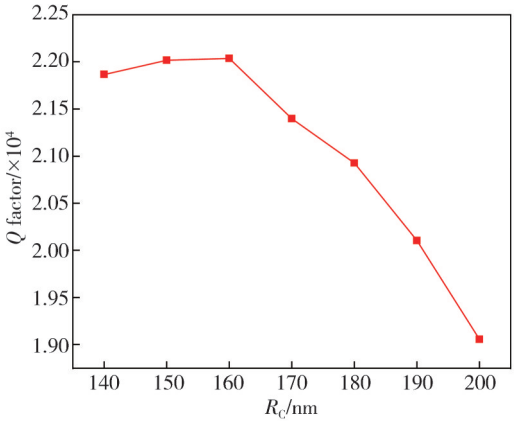

Fig. 10 Q factor at different R_C

Considering that there may be deviations when the aperture of the device is realized, and the errors introduced by the silicon-based material in the manufacturing process may have a certain impact on the sensing performance of the device, tolerance analysis of key dimensions is indispensable. On the basis of optimizing the relevant parameters, the influence of the aperture of the elliptical hole with different R_C and r_C on Q factor and extinction ratio of AFPSMRR in the fluctuation range of ±10 nm is analyzed. It can be seen from Fig. 11 that with the increase of the aperture of the elliptical holes, the Q factor and the extinction ratio increase first and then decrease. When the long axis radius R_C of the hole is in the range of 150 nm－170 nm, the minimum Q factor and the extinction ratio are 21 398 and 23.36 dB, respectively. With the fluctuation of the short axis radius r_C from 90 to 110 nm, Q factor and extinction ratio reach the minimum at r_C=100 nm, which are 21 642.8 and 23.63 dB, respectively. The device shows good stability and can maintain good performance within the process tolerance range.

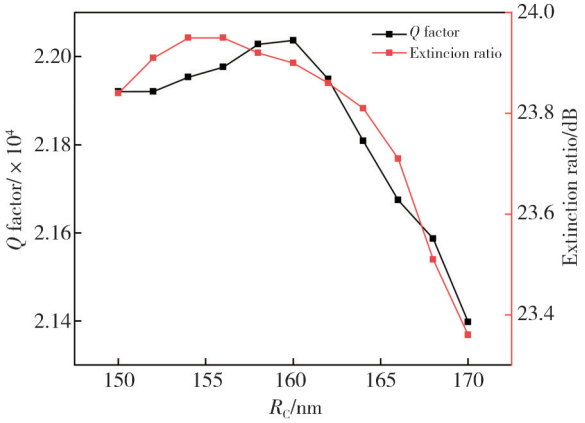

(a) Q factor and extinction ratio at different R_C

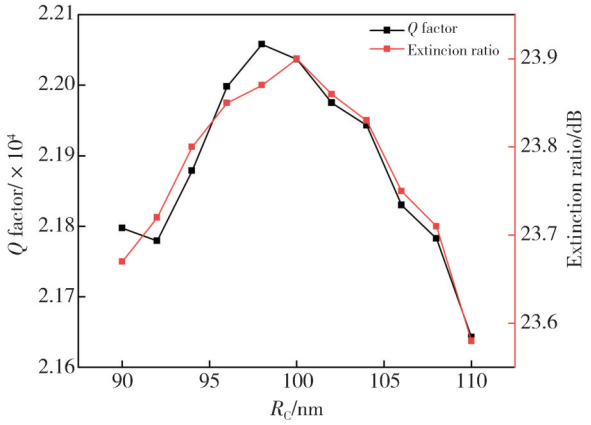

(b) Q factor and extinction ratio at different r_C

Fig. 11 Influence of R_C and r_C on Q factor and extinction ratio

3 Refractive index sensing characteristics

Based on the optimized structural parameters, the refractive index sensing characteristics of the device were analyzed by monitoring the shift of the resonant wavelength caused by the surrounding environment. In the simulation process, the device was placed in a solution containing biological analytes with refractive indexes of 1.333, 1.335, 1.337, 1.339, and 1.341, respectively. The simulated transmission spectrum is shown in Fig. 12(a). The change of the refractive index of the cladding layer will affect the interaction between the light mode in the structure and the external environment, as well as the effective refractive index.

In sensing applications, the sensitivity is expressed as

$$S=\frac{\Delta\lambda}{\Delta n}, \tag{13}$$

where Δn is the change of the effective refractive index, and $\Delta\lambda$ is the offset of the resonance wavelength. It can be seen from Fig. 12(b) that when n increases, the resonance wavelength shifts. The sensitivity reaches 354 nm·RIU^{-1}, and the limit of detection (LOD) is 2×10^{-4}RIU.

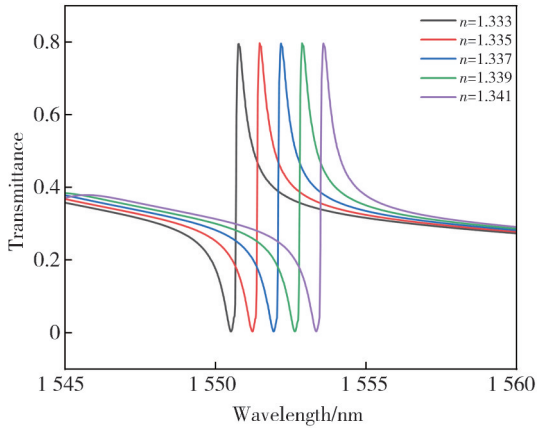

(a) Spectra at different environmental refractive indexes

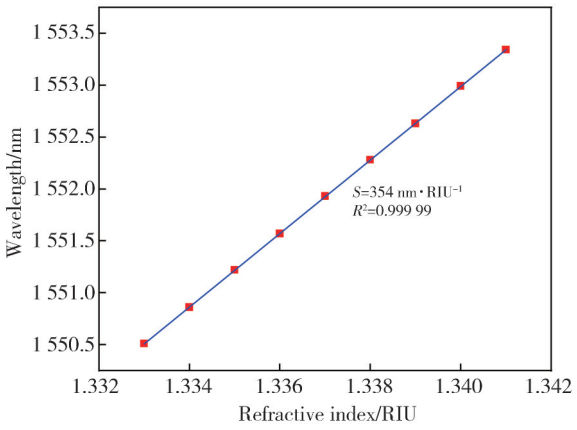

(b) Curve of wavelength variation with refractive index

Fig. 12 Analysis of refractive index sensing characteristics

In addition, the resonance wavelength has a good linear relationship with the refractive index, and the fitting rate exceeds 99%.

The structure is compared with slot-MRR proposed in other papers in terms of four parameters: Q factor, sensitivity, footprint and LOD. It can be seen from Table 1 that most of the devices proposed in the references have the problems of high sensitivity and low Q factor.

This is mainly because some devices may increase the loss of the device due to structural design, material properties, coupling methods and other reasons in the design process, making the Q factor of the device lower. The slot micro-ring resonator sensor with asymmetric FP cavity proposed has good sensitivity while ensuring high Q factor. And the footprint of the structure is smaller in the same order of LOD, in contrast, higher integration. Therefore, it has relatively obvious application potential in the field of biochemistry and many other fields.

Table 1 Comparison of refractive index sensing characteristics of MRR based on slot structure

Refractive index sensor	Q factor	S/(nm·RIU^{-1})	Footprint/μm^2	LOD/RIU
Ref.[25]	108 000	99.03	122	—
Ref.[26]	3 100	620	116	1.4×10^{-4}
Ref.[27]	16 000	563	1 286	3.7×10^{-6}
Ref.[28]	10 000	471	14 641	3.3×10^{-4}
Proposed structure	22 037.1	354	142	2×10^{-4}

4 Conclusions

In this work, a structure of a slot micro-ring resonator based on an asymmetric FP cavity was proposed. The reflection signal of the FP cavity formed by the elliptical holes acts as a continuous state light and interferes with the Lorentzian discrete state light generated by the MRR to produce Fano resonance. Since asymmetric Fano

resonance line shape has a larger slope, a higher Q factor can be obtained. If it is applied to the sensing, the small spectral shift caused by the change of refractive index in the environmental medium can be detected, thus forming a better detection limit, which has a significant advantage for improving the performance of the sensor. The working principle of the device was analyzed by the transfer matrix method, and the influence of different physical parameters on the performance of the device was simulated by FDTD. The results show that the Q factor of the slot micro-ring resonator based on the asymmetric FP cavity can reach 22 037.1, and the extinction ratio is 23.9 dB. In terms of refractive index sensing characteristics, its sensitivity can reach 354 nm/RIU. Therefore, the designed compact device is easy to integrate and can be applied to the sensing array, which has great potential in the field of optical sensing.

Acknowledgement

This work was supported by Natural Science Foundation of Gansu Province (No. 22JR5RA320).

Declaration of conflicting interests

The authors have no conflict of interests related to this publication.

References

[1] LIU L, HU Z H, YE M Y, et al. On-chip refractive index sensor with ultra-high sensitivity based on sub-wavelength grating racetrack micro-ring resonators and Vernier effect. IEEE Photonics Journal, 2022, 14(5): 6849007.

[2] ORCUTT J S, MOSS B, SUN C, et al. Open foundry platform for high-performance electronic-photonic integration. Optics Express, 2012, 20(11): 12222-12232.

[3] PETRUŠKEVIČIUS R, BALČYTIS A, URBONAS D, et al. Microring resonators with circular element inner-wall gratings for enhanced sensing. Japanese Journal of Applied Physics, 2020, 59(SO): SOOD02.

[4] CHEN H X, LIAO L J, ZHAO X, et al. High-sensitivity electrocardiogram sensor based on Fano resonance in a double-stub-assisted plasmonic micro-ring resonator. Optics & Laser Technology, 2024, 169: 109874.

[5] KUMAR VERMA Y, KUMARI S, MANI TRIPATHI S. Grating assisted temperature insensitive micro-ring resonator biosensor. Journal of Optics, 2023, 25(12): 125801.

[6] BRYAN M R, BUTT J N, BUCUKOVSKI J, et al. Biosensing with silicon nitride micro-ring resonators integrated with an on-chip filter bank spectrometer. ACS Sensors, 2023, 8(2): 739-747.

[7] FERNÁNDEZ BLANCO A, HERNÁNDEZ PÉREZ M, MORENO TRIGOS Y, et al. Development of optical label-free biosensor method in detection of listeria monocytogenes from food. Sensors, 2023, 23(12): 5570.

[8] BISWAS U, RAKSHIT J K, BHARTI G K. Design of photonic crystal micro-ring resonator based all-optical refractive-index sensor for analyzing different milk constituents. Optical and Quantum Electronics, 2019, 52(1): 19.

[9] GU L P, FANG H L, LI J T, et al. A compact structure for realizing Lorentzian, Fano, and electromagnetically induced transparency resonance lineshapes in a micro-ring resonator. Nanophotonics, 2019, 8(5): 841-848.

[10] ZHANG J F, LIANG L X, WU X S, et al. Research on output multiline micro-ring resonator. Acta Optica Sinica, 2023, 43(9): 212-219.

[11] ZHAO G L. Tunable Fano resonances based on micro-ring resonators. Lanzhou: Lanzhou University, 2018.

[12] XING E B, LI J L, RONG J M, et al. Fabrication of ultra-high optical quality factor crystalline resonator and prism coupling package. Journal of Test and Measurement Technology, 2022, 36(4): 277-280.

[13] FAN S H. Sharp asymmetric line shapes in side-coupled waveguide-cavity systems. Applied Physics Letters, 2002, 80(6): 908-910.

[14] WANG G C, SHEN A, ZHAO C Y, et al. Fano-resonance-based ultra-high-resolution ratio-metric wavelength monitor on silicon. Optics Letters, 2016, 41(3): 544-547.

[15] XU Y M, LI J X, KONG M. Various resonance lineshapes available in a single micro-ring resonator. Journal of Optics, 2021, 23(4): 045801.

[16] PENG F C, WANG Z R, YUAN G H, et al. High-sensitivity refractive index sensing based on Fano resonances in a photonic crystal cavity-coupled micro-ring resonator. IEEE Photonics Journal, 2018, 10(2): 6600808.

[17] GAO J, ZHANG D L, LU L D, et al. Fano resonator design and sensing characteristics research based on racetrack micro-ring resonator. Journal of Electronic Measurement and Instrumentation, 2021, 35(5): 24-30.

[18] LIU C J, SUN X L, WU X S, et al. Slot phase-shifting bragg grating micro-ring resonator and its sensing characteristics. Journal of Photonics, 2023, 52(6): 47-57.

[19] WEN Y J, SUN Y, DENG C Y, et al. High sensitivity and FOM refractive index sensing based on Fano resonance in all-grating racetrack resonators. Optics Communications, 2019, 446: 141-146.

[20] WU N X, XIA L. High-Q and high-sensitivity multi-hole slot micro-ring resonator and its sensing performance. Physica Scripta, 2019, 94(11): 115512.

[21] GU L P, FANG L, FANG H L, et al. Fano resonance lineshapes in a waveguide-micro-ring structure enabled by an air-hole. APL Photonics, 2020, 5(1): 5124092.

[22] LIMONOV M F, RYBIN M V, PODDUBNY A N, et al. Fano resonances in photonics. Nature Photonics, 2017, 11(9): 543-554.

[23] AVRUTSKY I, GIBSON R, SEARS J, et al. Linear

systems approach to describing and classifying Fano resonances. Physical Review B, 2013, 87(12): 125118.
[24] MCGARVEY-LECHABLE K, HAMIDFAR T, , PATEL D, et al. Slow light in mass-produced, dispersion-engineered photonic crystal ring resonators. Optics Express, 2017, 25(4): 3916-3926.
[25] YANG D Q, DUAN B, ZHANG X, et al. Nanoslotted micro-ring resonator for high figure of merit refractive index sensing. Optica Applicata, 2020, 50(1): 37-47.
[26] CHENG W Q, SUN X, YE S W, et al. Sidewall grating slot waveguide micro-ring resonator biochemical sensor. Optics Letters, 2023, 48(19): 5113-5116.
[27] CHENG W Q, SUN X, YE S W, et al. Double slot micro ring resonators with inner wall angular gratings as ultra-sensitive biochemical sensors. Optics Express, 2023, 31(12): 20034-20048.
[28] ZHANG X L, ZHOU C, LUO Y F, et al. High *Q*-factor, ultrasensitivity slot micro-ring resonator sensor based on chalcogenide glasses. Optics Express, 2022, 30(3): 3866-3875.

非对称法布里-珀罗腔槽型微环谐振器及其传感特性

曹倩倩, 刘春娟*, 吴小所, 孙晓丽

兰州交通大学 电子与信息工程学院, 甘肃 兰州 730070

摘　要: 为实现高品质因子和高灵敏度的折射率传感器, 提出了一种基于非对称法布里-珀罗(Fabry-Perot, FP)腔的槽型微环谐振器(Micro-ring resonator, MRR)。该结构中, 一对椭圆形孔构成的法布里-珀罗腔与微环谐振器形成两种不同的光模式, 因破坏性干涉而形成Fano线型, 由此获得了较高品质因子和消光比, 提高了系统灵敏度。利用传输矩阵法分析该结构的传输原理, 利用时域有限差分法仿真该结构的透射谱图及模场分布, 并对器件中影响Fano线型的关键结构参数进行了优化。结果表明, 该器件的品质因子可达22 037.1, 消光比为23.9 dB。采用折射率传感特性分析, 得到该结构的灵敏度为354 nm·RIU^{-1}, 灵敏度的检测极限为2×10^{-4}RIU。因此, 所提出的非对称法布里-珀罗腔槽型微环谐振器结构紧凑、性能优良, 在传感应用方面优势较为明显。

关键词: 微环谐振器; 法布里-珀罗腔; Fano共振; 折射率传感; 集成光学; 硅基波导

引用格式: CAO Qianqian, LIU Chunjuan, WU Xiaosuo, et al. Asymmetrical Fabry-Perot cavity slot micro-ring resonator and its sensing characteristics. Journal of Measurement Science and Instrumentation, 2024, 15(3): 292-301.